Arch. Metall. Mater., Vol. 61 (2016), No 2, p. 499–502

DOI: 10.1515/amm-2016-0087

K. GRUSZKA*, M. NABIAŁEK*, K. BŁOCH*,#

THE INFLUENCE OF HEAT TREATMENT ON THE MAGNETIZATION PROCESS (WITHIN STRONG MAGNETIC FIELDS) FOR THE ALLOY: $Fe_{61}Co_{10}Y_8Cu_1B_{20}$

Samples of $Fe_{61}Co_{10}Y_8Cu_1B_{20}$ alloy were investigated in the 'approach to ferromagnetic saturation' region by using the Kronmüller method. The amorphous material was obtained by radially cooling the molten alloy under a protective atmosphere of inert gas. Following this manufacturing process, static magnetic hysteresis loops were measured for samples, before and after a controlled isothermal annealing process, using a LakeShore vibrating magnetometer (VSM). From analysis of the primary magnetization curves, the distribution of structural defects and the average exchange distance for these defects were determined.

Keywords: bulk amorphous, Kronmüller method, XRD, structural defects

1. Introduction

Improvement of the properties of metallic alloys is one of the main objectives of modern physics and material sciences. The continuous increase in demand for cost-effective materials with good soft magnetic properties constantly drives many industries. To meet these requirements, extensive research is carried out in the production and processing of materials, in order to achieve very specific magnetic parameters [1-3]. Predominantly, in order to obtain alloys with good soft magnetic properties, the aim is to prepare materials featuring an amorphous structure [4-6]. To improve the properties of such materials, heat treatment is frequently used in order to bring about the relaxation of the structure; this leads to a reduction in the defects and stresses present [7-9]. Controlled heat treatment may also lead to the formation of small-sized grains in the material, reaching up to 100 nm in one dimension [10-11]. This process, called nanocrystallization, has a significant impact on the performance parameters of the obtained materials.

Within the structure of the material, defects have a significant impact on the process of magnetization in high magnetic fields [12-14]. In the case of crystalline materials, the definition of these defects does not cause more problems; however, in the case of amorphous materials, it is difficult to specify with clarity. In this case, to facilitate interpretation, a comparative method is used. Fig. 1 shows schematically two types of defects found in crystalline materials, together with their equivalents for amorphous materials.

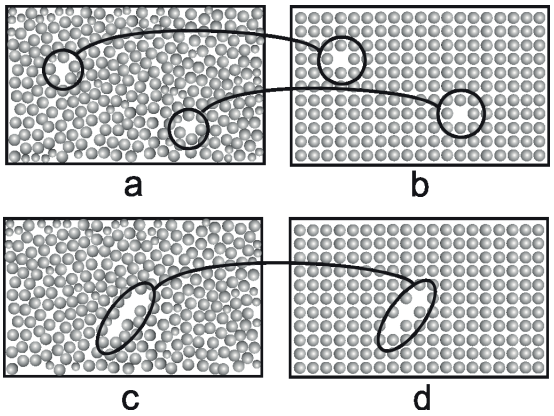

Fig. 1. Defects occurring in amorphous materials (a, c), and their crystalline equivalents (b, d).

In this paper, investigations on $Fe_{61}Co_{10}Y_8Cu_1B_{20}$ alloy samples are described, determining: (1) the influence of structural defects on the process of magnetization in high magnetic fields, and (2) the effect of controlled heat treatment on the magnetic properties.

2. Studied material

An ingot of alloy, of chemical composition $Fe_{61}Co_{10}Y_8Cu_1B_{20}$, was prepared using a plasma arc to melt the component substances; a protective gas atmosphere was used, at reduced pressure. The alloying elements were characterized by high purity (99.99%), and the ingot

* CZESTOCHOWA UNIVERSITY OF TECHNOLOGY, FACULTY OF PRODUCTION ENGINEERING AND MATERIALS TECHNOLOGY, INSTITUTE OF PHYSICS, 19 ARMII KRAJOWEJ AV., 42-200 CZESTOCHOWA, POLAND

Corresponding author: bloch@wip.pcz.pl

was mixed repeatedly, to ensure uniform distribution of the component substances throughout the volume of the material. Amorphous samples were prepared using the radial-cooling method. Under an atmosphere of protective gas (argon), the liquid alloy was injected into a water-cooled copper mould (injection casting). Two of the resulting amorphous samples were then subjected to a controlled heat treatment process at two different temperatures: 917 [K] (sample b) and 927 [K] (sample c) over time durations of 5 and 15 minutes, respectively. These temperatures were selected to be slightly below the crystallization temperature, from results previously obtained using differential scanning calorimetry (DSC). Next, with the help of X-ray diffraction (using a BRUKER D8 ADVANCE diffractometer, CuKα, 0.02°/step) structural studies of the produced alloys were performed, along with investigations into the magnetic properties of the samples, using a vibrating magnetometer (LakeShore, model 7301). The obtained SEM images were taken using Supra Zeiss firm Detector SE working with 20 kV acceleration voltage. Primary magnetization curve analysis was performed, according to the Kronmüller theory [15].

3. Results

Fig. 2 shows the X-ray diffraction pattern for a sample in the as-quenched state.

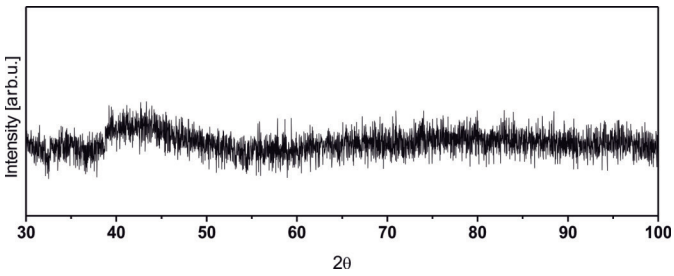

Fig. 2. The XRD diffraction pattern of a sample in the as-quenched state

The X-ray diffraction pattern, featured in Fig. 2,reveals only a single, wide, blurred maximum; this demonstrates an absence of long-range interactions, and thus the fully-amorphous nature of the sample. After the annealing process, undertaken at controlled temperatures of 917 [K] and 927 [K] for respective times of 5 and 15 minutes, the diffraction pattern was found to feature narrow, relatively intense, peaks of the crystalline phases identified as Fe_5Y, $Fe_{17}Y_2$ and α-Fe; this diffraction pattern is shown in Fig. 3.

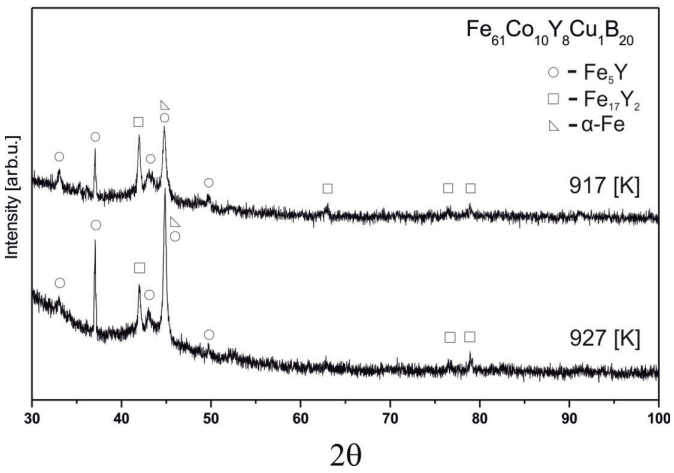

Fig. 3. The XRD diffraction pattern for samples in the state after isothermal annealing, at temperatures of 917 [K] and 927 [K]

Figure 4 and figure 5 are presenting SEM breakthroughs images of sample in state after solidification and in state after isothermal annealing in 927 [K] respectively.

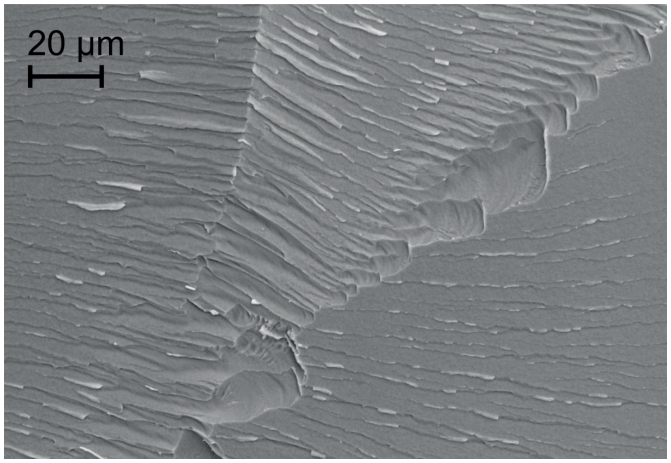

Fig. 4. SEM image of sample breakthrough in the as-quenched state

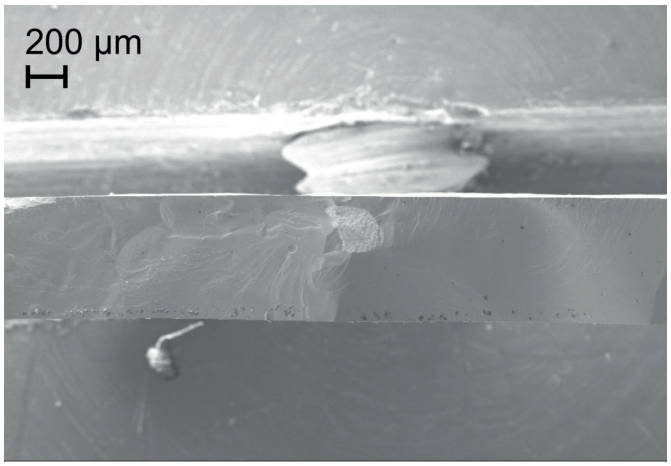

Fig. 5. SEM image of sample breakthrough in state after isothermal annealing in 927 [K]

As can be seen in fig. 4 the breakthrough consists of typical structures for amorphous material. The presence of husk structure passing thru vein-like breakthrough into smooth formation can be observed. The remaining part of sample shows mainly the smooth breakthrough type structure. After isothermal annealing both in 917 [K] and 927 [K] the SEM images of samples are similar in their character. The main part of those is consisting of smooth breakthrough passing to the vein like structure. In the samples treated by annealing process as a result of diffusion processes fragility can be increased due to the loss of plasticity in these regions. In figure 5 a white crystalline like structure with size of about 200 [μm] can be seen (in the middle of breakthrough). It was found that this structure is part of not mixed consistent material developed during the pre-melting procedure that did not appeared in other sample parts.

Next, static magnetic hysteresis loops were recorded for all of the investigated samples (figure 6).

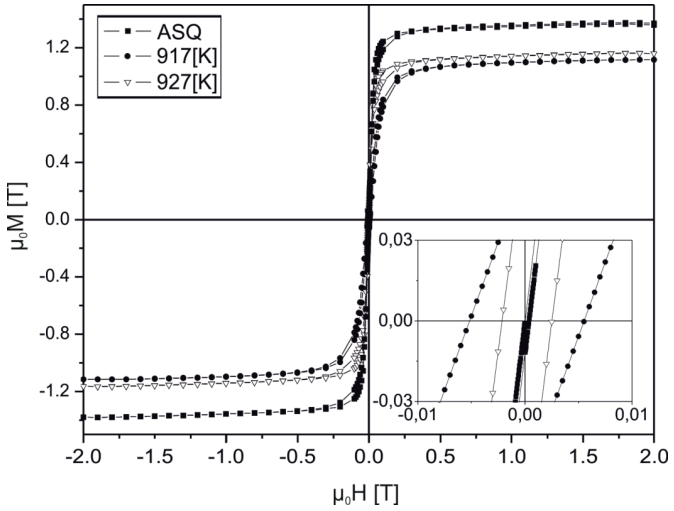

Fig. 6. Static magnetic hysteresis loops for the samples in the as-quenched state (ASQ), and annealed at 917 [K] and 927 [K]; also a close-up of the origin of the co-ordinate system μ_0M-μ_0H

Data gathered from the analysis of the static magnetic hysteresis loops are summarized in Table I.

TABLE 1
Some key parameters, obtained from analysis of the static magnetic hysteresis loops

Annealing temp. [K]	Magnetic saturation [T]	Coercivity field [A/m]
ASQ	1.36	139
917	1.11	4256
927	1.16	1550

As can be seen, a sampleannealedat917[K] exhibited the largest coercivity field. However, annealing at 927 [K] did not result in a further increase in the coercivity field. The increase in the coercivity field of the annealed samples is due to the appearance of grains of the semi-hard magnetic phases: Fe_5Y and $Fe_{17}Y_2$. Using the Rietveld refinement, the percentages of mutual phases were calculated (Table II). As can be seen, in the sample annealed at 927 [K], the ratio of phase Fe_5Y to phase α-Fe is much smaller than that for the sample annealed at 917 [K],where this proportion is similar.

TABLE 2
The mutual participation of crystalline phases

Annealing temp. [K]	Crystalline phase		
	α-Fe [%]	Fe_5Y [%]	$Fe_{17}Y_2$ [%]
917	49.10	46.68	4.22
927	67.91	28.49	3.60

Next, in accordance with the H. Kronmüller theory, analyses of the initial magnetization curves were conducted for all samples, using the relationship:

$$\mu_0 M(H) = \mu_0 M_S \left[1 - \frac{a_{1/2}}{(\mu_0 H)^{1/2}} - \frac{a_1}{(\mu_0 H)^1} - \frac{a_2}{(\mu_0 H)^2}\right] + b(\mu_0 H)^{1/2}, \quad (1)$$

Where: a_i and b are coefficients of the linear fits responsible for the occurrence of defects ($a_{1/2}$, a_1, a_2) and for the Holstein-Primakoff process (b). Fig. 7 shows the linear fit factor, responsible for the approach to the second law of ferromagnetic saturation. According to the H. Kronmüller theory, in the case of amorphous samples, it is possible to determine the type of defect that has the greatest impact on the process of magnetization in high magnetic fields. For the sample in the as-quenched state, a linear relationship of μ_0M versus $(\mu_0 H)^{-1}$ was observed over the range from 0.35 [T] to 0.53 [T]; for the same sample, linear defects were found to exert the dominant influence on the process of magnetization in high fields (Fig. 7). This is on the assumption that the size of the linear pseudo-dislocation dipole is less than the exchange distance ($D_{dip}<l_H$). Data obtained from analysis of the initial magnetization curves are summarized in Table 3.

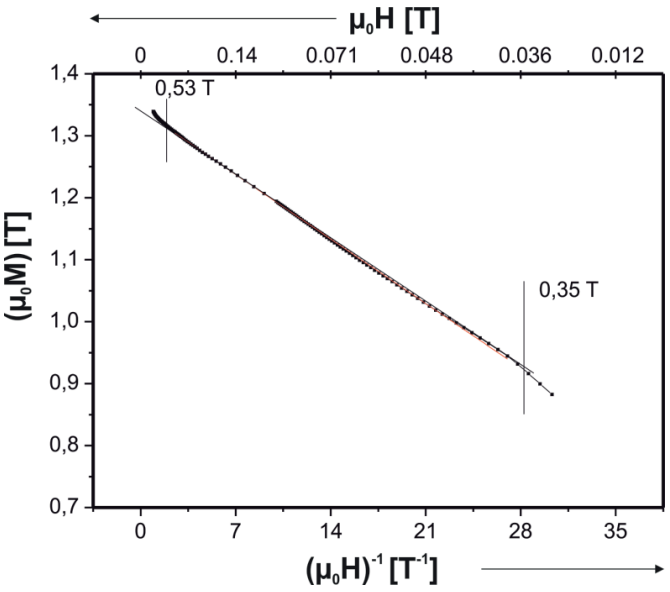

Fig. 7. Magnetization curve, as a function of $(\mu_0 H)^{-1}$, for the $Fe_{61}Co_{10}Y_8Cu_1B_{20}$ alloy in as-quenched state

For heat-treated samples, it is not possible to determine the dominant type of structural defect, as the Kronmüller theory

was developed only for single-phase materials. However, the process of magnetization at high fields, in addition to structural defects, is significantly affected by the Holstein-Primakoff process, which is associated with the suppression of thermally-excited spin waves. The linear fit coefficient b of this process can be described by:

$$b = 3.54\, g\, \mu_0 \mu_B \left(\frac{1}{4\pi D_{spf}}\right)^{3/2} k\, t\, (g\mu_B)^{1/2} \qquad (2)$$

where: D_{spf} - spin wave stiffness parameter, μB μ_B – Bohr's magneton, k – Boltzmann constant, g – gyromagnetic factor. Fig. 5 contains a linear fit for the suppression of thermally-excited spin waves.

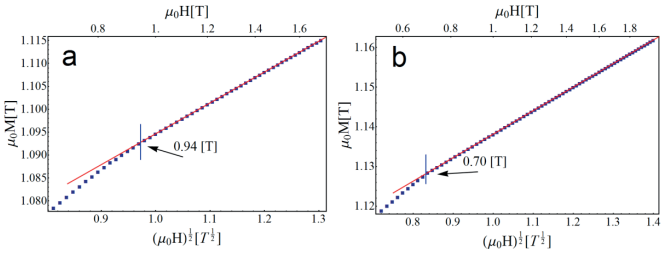

Fig. 8. Magnetization curve, as a function of $(\mu_0 H)^{1/2}$, for the samples annealed at 917 [K] (a) and at 927 [K] (b). The Holstein-Primakoff process

Table III. Data obtained from analysis of the initial magnetization curve; *b* - the coefficient of the linear fit for the Holstein - Primakoff process, D_{sp}- spin wave stiffness parameter.

TABLE 3

Data obtained from analysis of the initial magnetization curve; b - the coefficient of linear fit for the Holstein-Primakoff process, D_{sp}- spin wave stiffness parameter, A_{ex}- exchange constant, l_H- exchange distance, N_{dip}- defect surface density

State	a_1 [10^{-2} T^1]	b [10^{-2} $T^{1/2}$]	D_{sp} [10^{-2}meV nm^2]
ASQ	1.10	6.871	39.58
917	-	6.700	40.13
928	-	5.900	43.69

By analysing the results, shown in Table III, it can be seen that, in the case of heat-treated samples, an increase has occurred in the spin wave stiffness parameter. Such an increase in this parameter is associated with an increase in the local density of magnetic atoms.

4. Conclusions

The magnetic properties of the considered alloy sample can be modified through the application of a controlled process of isothermal annealing. A single-step annealing process, carried out at two different temperatures, is characterized by a different course of crystallization process dynamics, leading to a different distribution of phase percentages.

For an amorphous sample, linear conglomerates of point defects exert the predominant effect on the process of magnetization in strong magnetic fields. Since the spin wave anchoring centres usually are located near structural defects, it can be assumed that the quantity of defects was decreased in the isothermally- annealed samples.

Heat treatment of the alloy significantly affected the value of the spin wave parameter. The increase in the spin wave parameter for the heat-treated samples can be explained by the increased number of nearest magnetic atoms.

During the heating process, structural relaxations occurred; in the case of the investigated alloy, this resulted in a reduction in the distance between magnetic atoms. This improves the chemical short-range order.

REFERENCES

[1] M.G. Nabiałek, P. Pietrusiewicz, M.J. Dospiał, M.Szota, K. Błoch, K. Gruszka, K. Oźga, S. Garus, Journal of Alloys and Compounds **615**(S1), 51-55 (2014).

[2] K. Gruszka, M. Nabiałek, K. Błoch, J. Olszewski, Nukleonika **60**(1), 23-27 (2015).

[3] S. Lesz, R. Szewczyk, D. Szewieczek, Journal of Materials Processing Technology **157**(1), 743-748 (2004).

[4] A.Inoue, Materials Science and Engineering A 226-228 (1997).

[5] A. Inoue, ActaMaterialia **48**, 279-306 (2000).

[6] D. Szewieczek, S. Lesz, Journal of Materials Processing Technology **162**, 1, 254-259 (2005).

[7] Zhou Zheng, Qi Xing, Zhenxi Sun, Jing Xu, Zhengfeng Zhao, Shuying Chen, Peter K. Liaw, Yan Wang, Materials Science and Engineering: A **626**, 467-473 (2015).

[8] H. Chiriac, N. Lupu, Physica B **299**, 293-301 (2001).

[9] D Szewieczek, J. Tyrlik-Held, S. Lesz, Journal of Materials Processing Technology **109** 1-2, 190-195 (2001).

[10] T. Kulik, T. Horubała, H. Matyja, Materiale Science and Engineering A**157**, 107-112 (1992).

[11] T. Kozieł, A. Zielińska-Lipiec, Z. Kędzierski, T. Czeppe, Journal of Microscopy **224** ,27-29 (2006).

[12] G. Nguyen Vien, S. Rioual, F. Gloaguen, B. Rouvellou, B. Lescop, Journal of Magnetism and Magnetic Materials **401**, 378-386 (2016).

[13] K. Devi Chandrasekhar, S. Mallesh, J. Krishna Murthy, A.K. Das, A. Venimadhav, Physica B: Condensed Matter **448**, 304-311 (2014).

[14] Ján Füzer, Samuel Dobák, Peter Kollár, Journal of Alloys and Compounds **628**, 335-342 (2015).

[15] H. Kronmüller, Journal of Applied Physics **52**(3), 1859-1864 (1981).